

Development of a Q2MM Force Field for the Asymmetric Rhodium Catalyzed Hydrogenation of Enamides

Patrick J. Donoghue,[†] Paul Helquist,[†] Per-Ola Norrby,[‡] and Olaf Wiest^{*,†}

Department of Chemistry and Biochemistry, University of Notre Dame, Notre Dame, Indiana 46556-5670, and Department of Chemistry, University of Gothenburg, SE-412 96 Göteborg, Sweden

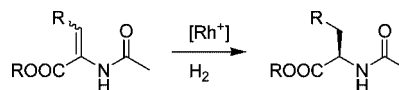
Received April 17, 2008

Abstract: The rhodium catalyzed asymmetric hydrogenation of enamides to generate amino acid products and derivatives is a widely used method to generate unnatural amino acids. The choice of a chiral ligand is of utmost importance in this reaction and is often based on high throughput screening or simply trial and error. A virtual screening method can greatly increase the speed of the ligand screening process by calculating expected enantiomeric excesses from relative energies of diastereomeric transition states. Utilizing the Q2MM method, new molecular mechanics parameters are derived to model the hydride transfer transition state in the reaction. The new parameters were based off of structures calculated at the B3LYP/LACVP** level of theory and added to the MM3* force field. The new parameters were validated against a test set of experimental data utilizing a wide range of bis-phosphine ligands. The computational model agreed with experimental data well overall, with an unsigned mean error of 0.6 kcal/mol against a set of 18 data points from experiment. The major errors in the computational model were due either to large energetic errors at high e.e., still resulting in qualitative agreement, or cases where large steric interactions prevent the reaction from proceeding as expected.

Introduction

The asymmetric hydrogenation of enamides has often been used in the synthesis of α -amino acids.¹ A representative example of this reaction is shown in Scheme 1. In order to perform this reaction asymmetrically, the choice of chiral ligand is essential but often left to trial and error. High throughput screening is often expensive both in cost of materials and in the time required to screen a large library. A computational method of ligand screening would be able to screen a large library of ligands quickly and without the need to purchase or synthesize the entire library ahead of time. A virtual library can also be more flexible than an experimental library as the virtual library can also include novel ligands that may not be immediately available. The ability to add new derivatives to the library or to design completely new ligands with a few mouse clicks makes the

Scheme 1. Rh-Catalyzed Hydrogenation of Enamides



virtual screening more robust than if the library were limited to previously synthesized ligands. Furthermore, since the bulk of the screening is done *in silico*, a large library could be screened by a single person without requiring an inordinate amount of time. This computational screening method would ultimately supplement the experimental screening by focusing the experimental screening on a smaller set of promising ligands. It is unlikely that any *in silico* screening method would be accurate in all cases. However, even with a small number of false negatives or false positives, the experimentalist would be led to a small set of useful ligands more efficiently than by current empirical methods.

A computational model of a metal catalyzed asymmetric reaction would have to involve a comparison of the energies of diastereomeric transition states. Specifically, this requires

* Corresponding author e-mail: owiest@nd.edu.

[†] University of Notre Dame.

[‡] University of Gothenburg.

calculating the $\Delta\Delta G^\ddagger$ of the diastereomeric transition states that lead to the enantiomeric products. In order to calculate the enantioselectivity of a reaction, a full conformational search of the stereoselecting transition state must be performed with the energies being derived from a Boltzmann distribution. An exhaustive Monte Carlo (MC) search of even a small molecule would be computationally impractical if done with quantum mechanical (QM) methods, especially in comparison to the time required to screen the library experimentally. Molecular mechanics (MM) methods offer a vast speed advantage over QM methods and implicitly include dispersive interactions, which are poorly described by single-determinant methods such as DFT, in their empirical parametrization of the nonbonded terms. However, MM methods do not have adequate parameters for most metals, nor are the underlying algorithms designed to determine local maxima on the potential energy surface (PES). Finally, the functional form used to describe bonds and angles is not designed to describe transition states involved in the forming and breaking of bonds, as there is no maximum point along these potentials. Transition states and transition metals are therefore typically calculated using the much slower QM methods. One solution to this problem is the use of a QM/MM model,² wherein the metal catalyst and any forming or breaking bonds that relate to the reaction coordinate are treated with QM, and the rest of the molecule is treated with MM. However, this still requires a QM calculation to be performed at each step in the MC search of the conformational space and can become computationally unfeasible. In order to maximize the speed advantage of MM over QM methods and to circumvent the well-known problems of the QM/MM cross terms,³ the model used to screen a large library should be purely MM in nature. To this end, this study employs the use of QM guided molecular mechanics or Q2MM. The Q2MM method derives MM parameters for any point on a PES, usually a transition state, from QM data and treats the state being modeled as a minimum by mathematically inverting the curvature along one dimension of the PES.⁴ While this method does require some selected QM calculations to be run, they are restricted to only the force field development and are not required for the actual library screening process.

The use of MM methods to model transition states has been fairly well established. As mentioned previously, MM methods cannot directly handle maxima on the PES, so early uses of MM methods used various ground state analogues for the transition state. To model the transition state of ester hydrolysis, DeTar and co-workers used an ortho-acid as a geometric model for the transition structure.⁵ More recently, a similar approach was used to determine structure-based activity of an enzyme through docking a transition state analogue to the enzyme.⁶ This type of approach assumes that energetic differences at the transition state are due to the steric nature of the surrounding environment and not due to the energy involved in the reaction coordinate itself.⁷ However, not all transition states do have appropriate ground-state analogues. To circumvent this, Houk and co-workers calculated transition states using *ab initio* methods and then utilized the fixed geometry of the breaking and forming

bonds in MM calculations to determine selectivity in reactions.⁸ This method ignores the possibility of the surrounding environment playing a role in the transition state geometry. While ground-state analogues would not respond to external forces the same way that real transition structures would, the ground-state analogues are still fully optimized structures. Houk followed this up by developing new parameters to model the transition state geometry as an energy minimum, thus making a transition state force field (TSFF). Bond lengths and angles of the new parameters were set to QM derived values, and the force constants were manually determined to reproduce MP2 energies.⁹ Menger criticized the validity of these force fields, suggesting that the observed trends by Houk and co-workers was due to ground-state interactions which could be better modeled by existing parameters,¹⁰ and then suggested an alternative method that could increase the efficiency of developing new parameters for future work.¹¹

The Goddard group has developed a unique method of MM, ReaxFF, wherein energy is not determined through explicit bonds but through bond orders based on atomic distances.¹² In other MM type calculations, the energy is based on the bonding specified by the input. Energies at transition structure geometries would be abnormally high, since the geometry is highly distorted from the expected ground-state geometry. ReaxFF determines bonding based on distance between atoms; therefore, a specific bonding scheme is not fixed throughout a single calculation. While this has been used for molecular dynamic simulations involving reactions,¹³ the optimization algorithms are still not designed to specifically locate transition states. The SEAM method, developed by Jensen, determines transition structures at the intersect of the reactant PES with the product PES.¹⁴ This method requires only ground-state parameters from which the transition state is extrapolated using Morse potentials in specialized software.

All of the previous methods are still reliant on existing parameters, but transition metal parameters are generally not available, although the ReaxFF force fields have included some metal parameters.¹⁵ Some attempts have been made to develop parameters for all elements, most notably in the UFF force field.¹⁶ Transition metal parameters, however, must take into account changes in the coordination sphere, and therefore general parameters may not be appropriate in all situations.

The Q2MM method is designed to avoid some of these shortcomings. The general philosophy behind this method is to rapidly create a reaction specific force field, thus trading the generality of a force field to achieve higher accuracy while maintaining the speed advantage of a MM method. The new parameters are derived from QM data and are designed to be specific to the reaction being studied.⁴ The transition structure is treated as a minimum and fully optimized similar to Houk's later work,⁸ but the force constants are derived from a modified Hessian matrix from the QM calculations.⁴ This approach circumvents the problems in the MM optimization algorithms that prevent optimization to transition structures by effectively reducing the dimensionality of the problem, and the highly specific

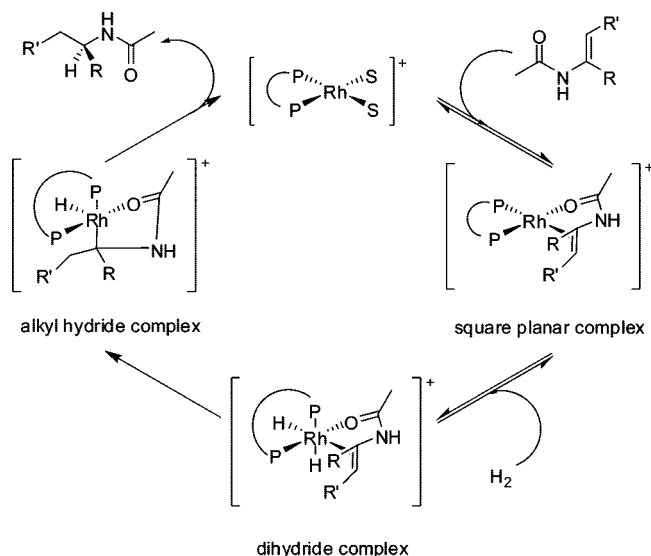


Figure 1. Overall mechanism of rhodium-catalyzed hydrogenation of enamides.

new parameters are able to describe the transition metal and transition structure appropriately.¹⁷

In order to develop a computational model for the asymmetric, rhodium catalyzed hydrogenation of enamides, the mechanism of the reaction must be known so that the correct stereodifferentiating transition states for the reaction are modeled. There has been a considerable amount of experimental^{18–21} and theoretical^{22,23} work done previously to determine the important transition states in the reaction. The overall reaction scheme is shown in Figure 1.

The substrate binds to the catalyst to form a square planar substrate-catalyst complex. This is followed by oxidative addition of H₂ to the complex to presumably form an octahedral dihydride species, although this species has not been observed experimentally. Transfer of one of the hydrides to the substrate yields an alkyl hydride complex that can be observed at low temperatures.¹⁸ Transfer of the second hydride to the substrate yields the product, which dissociates and regenerates the catalyst. The most notable feature of the asymmetric reaction is that the relative energies of the initial square planar catalyst-substrate complex do not correlate with the observed enantiomeric excess in the product. Specifically, the major diastereomeric square planar complex gives rise to the minor enantiomer of the product. The observed enantioselectivity is based on the relative reactivity of the two substrate-catalyst complexes with hydrogen to generate the product. This anti-lock-and-key mechanism is a distinguishing feature of the reaction.¹⁸ It has also been observed that formation of the alkyl hydride species after the first hydride transfer is irreversible.²¹

Previous computational studies have further elaborated on the mechanism of the reaction.^{22,23} There are four possible orientations of hydrogen addition to the square planar substrate-catalyst complex, as shown in Figure 2. Two of these paths, labeled B and D in the nomenclature used by Landis and co-workers,^{22a,b} involve the hydrogen adding parallel to the P–Rh–O bond, as opposed to the orthogonal P–Rh–alkene bond. Addition along these pathways has been determined to involve a very high barrier, and only the A

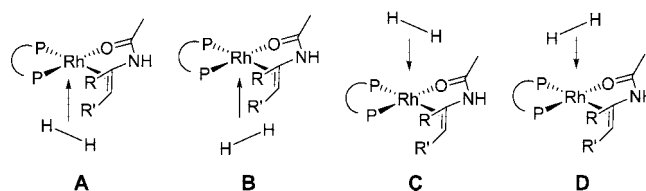


Figure 2. Mechanistic pathways derived from the orientation of H₂ addition.

and C pathways, adding the hydrogen parallel to the P–Rh–alkene bond, would be mechanistically accessible. The A and C pathways differ in the addition of hydrogen to the substrate based on proximity. Along the A pathway, the first hydride addition is made to the β -carbon of the substrate, distal to the enamide, while on the C pathway, the first hydride addition is made to the α -carbon, proximal to the enamide. Other studies from our laboratory²³ and others²² have identified that the bias for A and C pathways is based on the electronics of the substrate. For dehydro- α -amino acids, the A pathway is the only energetically feasible pathway for the reaction. If the substrate is electronically reversed to a dehydro- β -amino acid, the C pathway is the only energetically feasible pathway.²³ This is due to the anion stabilizing ability of the substrate at the transition state due to the location of various electron withdrawing groups. Due to the change in hydrogen addition as mentioned before, the alkyl hydride intermediate that can be observed at low temperatures should reflect this difference. Experimental studies have confirmed this regioselectivity in that only the A pathway alkyl hydride is observed for dehydro- α -amino acid substrates^{18a} and the C pathway alkyl hydride is observed for dehydro- β -amino acid substrates.^{18b}

The previous computational studies also identified the relative energies of the transition states between the square planar substrate-catalyst complex and the formation of the alkyl hydride species. The two key transition states involved are the oxidative addition of H₂ to form the dihydride species and the first hydride transfer to form the alkyl hydride intermediate. For the dehydro- α -amino acid substrates, these two transition states are close in energy, although the second transition state is generally slightly higher in energy. Coupled with the experimental studies that identify the formation of the alkyl hydride species to be irreversible, this study focuses solely on the second transition state as the key transition state to model for this reaction. As previously mentioned for the dehydro- α -amino acids studied here, only the A pathway is energetically feasible, and consequently there is only one transition state that needs to be modeled in this reaction, despite the complexity of the mechanism.

In the present manuscript, we will present the development of a Q2MM force field for the Rh(I)-catalyzed hydrogenation of enamides.⁴ First, a QM training set has been calculated, determining selected transition structures along with the corresponding Hessian matrices and partial charges. Second, we will discuss the adaptation of the basic force field, in this case MM3*, to include any missing parameters so that the force field can be used to describe the structures calculated via QM. This will be followed by a description of the optimization of the new force field parameters in stages

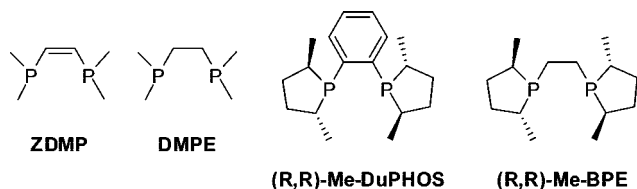


Figure 3. Ligands used for the QM training set.

to reproduce the QM data. Fourth, and finally, the new parameters are validated by calculation of experimentally observed enantiomeric excesses. Analysis of errors between theory and experiment can help further refine the force field parameters in an iterative way.

Computational Details

All QM calculations were performed using Jaguar 5.5²⁴ with all structures fully optimized at the B3LYP level of theory using the LACVP** basis set. This basis set corresponds to a combination of the Los Alamos double- ζ LANL2DZ ECP²⁵ for rhodium and the 6-31G** basis set for all other atoms. This basis set is identical to that used by our laboratory previously in mechanistic investigations²³ of the reaction and similar to that used by Landis and co-workers in both DFT^{22a} and ONIOM,^{22b,22c} level computations previously reported. All reported energies are enthalpies calculated at 298 K and 1 atm. Transition structures were located through the eigenvector following routine implemented in Jaguar and were confirmed as transition structures through the calculation of frequencies and identification of exactly one negative eigenvalues in the Hessian matrix. Partial charges were calculated through electrostatic potential fitting.²⁶ Molecular mechanics calculations were performed with MacroModel 8.6²⁷ using the MM3* force field as a functional form,²⁸ supplemented with additional terms as derived using the Q2MM method as described in the text and elsewhere.⁴ Enantiomeric excesses were calculated from Boltzmann weighted energies at 298 K calculated through Monte Carlo conformational search of the transition structure. At least 15000 MC steps were used for each diastereomer of each ligand-substrate combination, with additional 15000-step searches performed, if necessary, until the MC search had converged. MC searches were considered converged when no new low energy structures (within 1 kcal/mol of the global minimum) were located within the last 5000 steps of the search. Details of the input files used are given in the Supporting Information.

Results and Discussion

Calculation of the QM Training Set. The QM training set for this system is composed of four ligands in the respective diastereomeric transition structures in several conformations. All systems were calculated using the previously studied α -formamidoacrylonitrile as a model substrate for a dehydro-amino acid.^{22,23} The ligands used, shown in Figure 3, are comprised of two achiral ligands, Z-dimethylphosphinoethene (ZDMP) and dimethylphosphinoethane (DMPE), and two chiral ligands, (R,R)-Me-DuPHOS and (R,R)-Me-BPE. The two chiral ligands were calculated in

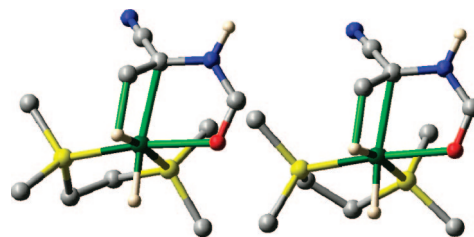


Figure 4. Optimized QM structures for the hydride transfer transition state using the DMPE ligand.

Table 1. Average Bond Lengths for Select Parameters in the Transition Structures

bond	av length (Å)	std. dev.
Rh–O	2.22	0.005
Rh–C	2.34	0.017
Rh–P _t	2.29	0.011
Rh–P _c	2.39	0.012
Rh–H _a	1.56	0.002
Rh–H _e	1.63	0.010
C–C	1.42	0.001
C–H	1.71	0.020

Table 2. Average Angles for Select Parameters in the Transition Structures

angle	av value (°)	std. dev.
O–Rh–C	74.6	0.411
O–Rh–P _t	171.4	2.608
O–Rh–P _c	89.7	0.894
O–Rh–H _a	93.0	1.074
O–Rh–H _e	93.0	0.790
C–Rh–P _t	113.6	3.076
C–Rh–P _c	108.1	3.146
C–Rh–H _a	162.1	1.180
C–Rh–H _e	83.0	1.006
P _t –Rh–P _c	86.4	0.354
P _t –Rh–H _a	79.2	2.098
P _t –Rh–H _e	89.5	0.495
P _c –Rh–H _a	84.2	2.532
P _c –Rh–H _e	168.8	4.162
H _a –Rh–H _e	84.9	1.902
C–C–H	117.4	0.709

both the *pro-R* and *pro-S* orientations of the dehydroamino acid. The two ligands with saturated backbones, DMPE and BPE, can undergo a pseudo ring flip when bound to the rhodium catalyst. This allows for a conformational change that adds an additional relative energy data point. In total, nine QM transition structures were calculated: one ZDMP structure, two DMPE conformations, two DuPHOS diastereomers, and two conformations of each of two BPE diastereomers.

The calculated QM structures showing the conformational switch in the DMPE ligand are shown in Figure 4. The BPE ligand undergoes a similar conformational change due to the saturated carbon linker between the two phosphorus atoms. The nine structures have very similar geometries around the rhodium catalyst and substrate. The average bond lengths and angle measurements of the structures involving the rhodium catalyst or forming and breaking bonds are shown in Table 1 for the bonds and Table 2 for the angles. A more complete table of geometric data, as well as Cartesian coordinates, is listed in the Supporting Information. The nine

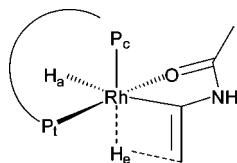


Figure 5. Rhodium catalyst and core atoms with labels used in the text.

calculated transition structures share structural similarities, with all bond lengths and angles involving the rhodium catalyst, and the changing bonds are fairly consistent between all nine structures. The substrate binding to the rhodium shows an almost constant Rh–O bond length with an average of 2.22 Å, but the Rh–C bond length shows some variation based on the size of the ligand. The Rh–C bond length for the two achiral ligands averages 2.32 Å. However, the larger DuPHOS and BPE ligands have the Rh–C bond length slightly longer at an average of 2.35 Å, for an overall average of 2.34 Å. The ligand binds asymmetrically to the rhodium catalyst with two different Rh–P bond lengths. For clarity, the two phosphorus atoms have been named P_c and P_t , with the phosphorus proximal to the oxygen denoted as P_c and the distal phosphorus as P_t . These labels are shown in Figure 5. The Rh– P_c bond has been calculated to have a length approximately 0.1 Å longer than the Rh– P_t bond, with average bond lengths of 2.39 Å and 2.29 Å, respectively, in good agreement with the large *trans* influence of hydrides compared to neutral oxygen ligands.^{19a,29}

The two hydrides bound to the Rh are also differentiated since the one in the phosphine plane is involved in the reaction coordinate. The reacting hydride in the equatorial plane of the phosphine ligand is labeled H_e , and the unreactive hydride that is out of the phosphine plane is labeled H_a and also described in Figure 5. The equatorial hydride has an expected longer average Rh–H bond distance of 1.63 Å compared to the average 1.59 Å for the axial hydride. The equatorial hydrides are also differentiated based on the size of the ligand as well. The achiral ligands have an average R– H_e bond length of 1.64 Å, whereas the larger chiral ligands have a slightly shorter Rh– H_e bond length of 1.62 Å. Furthermore, the forming C–H transition state bond length is slightly shorter for the achiral ligands, averaging 1.69 Å, whereas the chiral ligands have an average C–H bond length of 1.72 Å. This combination of data suggests that the larger steric demands of the chiral DuPHOS and BPE ligands enforce a slightly earlier transition state than the smaller achiral model ligands. Interestingly, the reacting C=C double bond does not show a noticeable bond length difference between the structures, with a 1.42 Å bond length for all calculated structures.

Modification of the MM3* Force Field. The existing MM3* force field supplied with MacroModel is insufficient to describe this transition state because it lacks suitable atom types and molecular mechanics parameters. As mentioned previously, the rhodium atom is not defined in the force field file. In addition to this, the existing parameters for hydrogen atoms are not sufficient for describing the two hydrides in the structure, and the two phosphorus atoms need to be differentiated. MacroModel includes a Z0 atom type that is

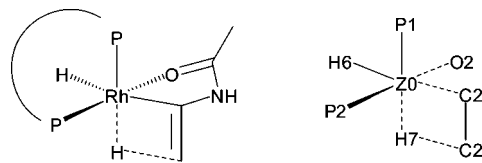


Figure 6. Substructure specification for new MM parameters. The overall structure is shown on the left, and the corresponding new atom types are shown on the right. All bonds in the substructure are single bonds, except for dashed bonds which are defined as zero order.

Scheme 2. Penalty Function for New MM Parameter Optimization

$$X^2 = \sum_i w_i^2 (y_{iQM} - y_{iMM})^2$$

designed for user definition; this atom type was used for the rhodium. The two hydrides were defined as atom types H6 (axial) and H7 (equatorial), which were amended to the atom type files as atom type numbers 46 and 47, respectively. The existing parameters for phosphorus atoms, previously labeled P0, were used in the creation of two more phosphorus atom types numbered 104 and 105, labeled as P1 and P2, and were not further optimized. The phosphorus proximal to the oxygen of the substrate was defined as being atom type P1, and the phosphorus distal to the oxygen was defined as atom type P2. The new parameters were then added to the force field file with the use of the substructure section that is utilized in MacroModel. The labeling of the substructure and given bonds are shown in Figure 6.

New MM Parameter Optimization. The newly defined parameters were optimized through the minimization of the penalty function, as described above and in Scheme 2. In the penalty function, the weighting values are the inverse of the tolerance for each type of data. The geometric tolerances are initially set to 0.01 Å for bonds, 0.5° for angles, and 1° for torsions. The tolerance for partial charges is set at 0.02 electrons. Various tolerances are used for the Hessian matrix to emphasize important interactions, like 1,4-interactions, while reducing the impact of longer range interactions. The tolerance for relative energies was initially set at 1 kJ/mol, but this tolerance was lowered to 0.1 kJ/mol to increase accuracy, as described later in the text. The minimization of the penalty function was performed through a combination of a Newton–Raphson and Simplex optimizations. The Simplex procedure is more efficient when the penalty function is far from a minimum, and therefore this is only used at early stages of the optimization. The optimization of the penalty function is considered converged when the function is improved by less than 0.01% between steps, with only Newton–Raphson steps used when the function improvement is less than 1% between optimization steps.

Initial bond lengths and angle measurements for parameters to be optimized were set to average QM values of the corresponding parameter, and the force constants were set to initial values of 5.0 mdyn/Å for bonds and 0.5 mdyn Å/rad² for angles. The definition of this substructure and added parameters for new atom types are given in the Supporting Information. The optimization of the new pa-

rameters was then undertaken in several steps. The first step was the optimization of the dipole moments in the new bond parameters to fit the partial charges of the MM structures to the calculated electrostatic potential (ESP) charges of the DFT structures. During this optimization, the only parameters optimized were the dipole moments, and the reference data were only the partial charges. Once the penalty function had converged for the dipole optimization, the next step of the optimization was the initial optimization of the force constants, which was done independently for each structure. In this step, only the force constants were optimized, with the penalty function convergence criteria set to 1% overall instead of 0.01%, and the comparison data in the penalty function were based on the geometric data and the full Hessian matrix for each structure independently.

After this optimization, it was noted that several force constants tended to zero consistently among all nine structures. Some other force constants were noted to be very large. These large values corresponded to forming or breaking bonds. Since the Hessian matrix was altered to change the single negative eigenvalue to a large positive value, this generates an artificially large force constant corresponding to the reaction coordinate.⁴ Therefore, these large force constants were allowable as long as they were involved in forming or breaking bonds. A single force field was then generated based on the optimized parameters for a better "initial guess" of force constants. These parameters were then optimized to reproduce the geometrical data of all nine structures along with the Hessian matrices of the achiral ligands and the relative enthalpies of diastereomeric structures. This optimization was done in two steps. First, the force constants alone were optimized with a 1% tolerance for convergence in the penalty function. Second, all geometric parameters and force constants were optimized with a 0.01% tolerance in the penalty function for convergence. In order to emphasize the importance of the relative energies in the parametrization, two force fields were derived from the QM data. The first force field, denoted as RhH, has the energy tolerance set at 1 kJ/mol for the relative energies. The second force field set the penalty threshold at 0.1 kJ/mol or a 10 times higher weighting for the error in the parametrization. This force field is denoted as the RhH-E. The resulting new parameters are listed in the Supporting Information. The bond lengths, angles, and force constants are given to four decimal places because of the number of significant figures required by the MacroModel program and is not meant to imply the level of accuracy of the parameters themselves.

The new bond parameters show excellent agreement with the average QM values for the corresponding bonds, as shown in Table 3 for the RhH and the RhH-E force fields, respectively. Furthermore, the bond parameters between the RhH and RhH-E force fields are extremely similar. The Rh–O bond length in the QM calculations had an average length of 2.22 Å. The new parameters for the Rh–O bond are 2.2213 Å for the RhH force field and 2.2091 Å for the RhH-E force field. The force constants for both fields are also similar, being 1.7982 and 1.7138 mdyn/Å, respectively. The average QM Rh–C bond length is 2.34 Å, and both

Table 3. New Bond Parameters for the RhH and RhH-E Force Fields

bond	RhH		RhH-E	
	length (Å)	force constant (mdyn/Å)	length (Å)	force constant (mdyn/Å)
Rh–P _c	2.3921	5.1238	2.3914	5.0700
Rh–P _t	2.2844	3.6079	2.2886	1.5293
Rh–O	2.2213	1.7982	2.2091	1.7138
Rh–C	2.3388	0.0000	2.3388	0.0000
Rh–H _e	1.6009	1.8394	1.6169	1.6059
Rh–H _a	1.5642	2.5618	1.684	2.5782
C–C	1.4317	5.5008	1.4281	4.1874
C–H	1.7686	18.4542	1.7492	21.9463

force fields have optimized parameters of 2.3388 Å, which is the actual average bond length when taken out to four decimal places. This parameter was not actually optimized, as the force constant for this bond was set to zero from the initial force constant optimization of each individual structure, as noted above. The parameter could not simply be omitted or the program would crash due to a missing parameter, even if that parameter does not contribute to the total energy due to the zero force constant. The Rh–P bonds were different based on their orientation to the substrate. The Rh–P_c bond length is 2.39 Å, and the Rh–P_t bond length is 2.29 Å in the QM structures. The force constants for the two bonds also varied slightly based on position and optimization procedure. The corresponding force field parameters were 2.3931 Å and 2.3914 Å, for the RhH and RhH-E force fields, respectively, for the Rh–P_c bond and 2.2844 Å and 2.2886 Å for the Rh–P_t bond. For the Rh–P_c bond, the two force fields had similar force constants, 5.1238 and 5.0700 mdyn/Å for the RhH and RhH-E force fields, respectively. The Rh–P_t had a force constant of 3.6079 mdyn/Å for the RhH force field but a weaker 1.5293 mdyn/Å for the RhH-E force field.

The two Rh–H bonds were also differentiated, with the axial, unreacting Rh–H bond being a slightly shorter 1.56 Å compared to the 1.63 Å of the reacting Rh–H bond. The parameters for the axial Rh–H bond were 1.5642 Å and 1.5684 Å, and for the reactive Rh–H bond the parameters were 1.6009 Å and 1.6169 Å for the RhH and RhH-E force fields, respectively. The force constants for the axial Rh–H bond were also larger than those for the equatorial Rh–H bond. In the RhH force field, the force constants were 2.5618 mdyn/Å for the axial bond and 1.8394 mdyn/Å for the equatorial bond, and in the RhH-E force field they were a similar 2.5782 and 1.6059 mdyn/Å.

The new parameters for the reacting C=C double bond are 1.4317 Å for the RhH force field and 1.4281 Å for the RhH-E force field, compared to an average value of 1.42 Å in the QM structures. This bond length suggests that the reacting C=C double bond is much more like a C–C single bond. The existing parameters for C–C single and double bonds utilizing the sp² hybridized C2 atom type in the MM3* force field have bond lengths of 1.3430 Å for a double bond and 1.4700 Å for a single bond. The force constant for the reacting C=C double bond was optimized to be 5.5008 mdyn/Å in the RhH force field and 4.1874 mdyn/Å in the

Table 4. Select New Angle Parameters for the RhH Force Field

angle	RhH		RhH-E	
	angle (°)	angle (°)	force constant (mdyn Å/rad ²)	force constant (mdyn Å/rad ²)
O–Rh–C	82.4448	71.8505	0.0009	0.0009
O–Rh–P _t	175.3066	169.9754	0.1113	0.1161
O–Rh–P _c	90.3323	90.4351	0.6735	0.6365
O–Rh–H _a	92.4769	93.0980	0.2785	1.2412
O–Rh–H _e	92.4818	92.2411	0.9752	0.9907
C–Rh–P _t	114.0324	113.9045	0.8134	1.2435
C–Rh–P _c	107.8407	108.8086	0.1108	0.1934
C–Rh–H _a	167.8640	168.5483	0.3168	0.2779
C–Rh–H _e	85.8487	85.5483	0.5178	0.8171
P _t –Rh–P _c	85.8789	86.0062	5.5794	4.7580
P _t –Rh–H _a	80.6824	84.3121	0.5802	0.4871
P _t –Rh–H _e	89.4721	89.4721	0.0000	0.0000
P _c –Rh–H _a	86.5384	85.4339	0.6378	0.7558
P _c –Rh–H _e	168.7540	168.7540	0.0000	0.0000
H _a –Rh–H _e	84.8617	84.8617	0.0000	0.0000
C–C–H	113.3287	113.3287	0.0000	0.0000

RhH-E force field. Both of these force constants are lower than for the existing ground-state bonds, being 7.5000 and 6.0000 mdyn/Å for double and single bonds, respectively.

The forming C–H bond has an average QM length of 1.71 Å, but the new values are slightly longer at 1.7686 Å for the RhH force field and 1.7492 Å for the RhH-E force field. The larger chiral ligands showed slightly longer C–H bonds at the transition states, and these larger parameters do not penalize this sterically larger environment for forcing a slightly earlier transition state. The force constant for this parameter is also rather large, 18.4542 mdyn/Å in the RhH force field and 21.9463 mdyn/Å in the RhH-E force field. However, this is an expected result of the Hessian inversion technique used in the Q2MM method. The negative eigenvalue of the Hessian matrix was replaced with a large positive value.⁴ Therefore, the force constants corresponding to the reaction coordinate will be unnaturally large as a result. Interestingly, only the forming C–H bond contains an abnormally large force constant, and the reacting C=C double bond and the breaking Rh–H bonds show force constants that are within the normal range for other parameters in the MM3* force field. Since the large force constant corresponds to the reaction coordinate, this suggests that the reaction coordinate is localized in this forming C–H bond and is not coupled to a corresponding C–C bond change or Rh–H bond breaking. Analysis of the QM calculated frequencies confirms this, with the negative frequency affecting almost exclusively the forming C–H bond.

There were also 22 new angle parameters optimized in the process. As with the bonds, the angle parameters were similar between the two force fields. Selected parameters are shown in Table 4 for the RhH and RhH-E force fields. The entire set of new parameters is listed in the Supporting Information. Out of these, four parameters had force constants set to zero after the initial individual parameter optimization. As with the Rh–C bond parameter, the angle parameters with zero force constants could not be omitted from the force field to allow for the program to run correctly. These parameters were the angles from the reacting, equatorial hydrogen to both phosphorus atoms, the angle between

the two hydrides on the rhodium, and the C–C–H angle of the substrate and reacting hydride. A fifth angle, the O–Rh–C angle, from the carbonyl oxygen to the α carbon of the substrate, had force constants that optimized to an extremely small 0.0009 mdyn Å/rad² for both force fields. The angle parameter for the O–Rh–C angle optimized to 82.4448° in the RhH force field and 71.8505° in the RhH-E force field. Compared to the average QM value of 74.6°, these optimized parameters are not in complete agreement. Since the O–Rh–C angle is part of a five-membered ring, and since the corresponding force constant is extremely low, the MM calculated angle can be defined through other parameters in the ring without a large energy penalty resulting from this discrepancy. This parameter could also be reset to the average QM angle with a zero force constant, as with the other four angles with zero force constants, but this is unnecessary since parameters with zero force constants do not affect the overall energy of the system.

The positioning of the carbonyl oxygen with respect to the phosphine ligand is determined through two O–Rh–P angle parameters corresponding to the two differentiated phosphorus atoms. The O–Rh–P_c angle was calculated to be 89.7°, and the optimized parameters are 90.3323° for the RhH force field and 90.4351° for the RhH-E force field. The O–Rh–P_t angle was calculated to be 171.4°, and the optimized parameters are 175.3066° for the RhH force field and 169.9754° for the RhH-E force field. Since the oxygen has a larger steric interaction with P_c, the agreement is more important with P_c than P_t. Furthermore, the corresponding force constants are higher for the O–Rh–P_c angle than for the P_t angle. The RhH force field has force constants of 0.6735 mdyn Å/rad² and 0.1113 mdyn Å/rad², for O–Rh–P_c and O–Rh–P_t, and the RhH-E force field has very similar values of 0.6365 mdyn Å/rad² and 0.1161 mdyn Å/rad².

The P–Rh–P ligand bite angle is also important in this system. Since the ligands were all bis-phosphine ligands with two carbon linkers, the bite angles of all the ligands were similar with an average 86.4° with very little variation between the QM calculated structures. The optimized MM parameters of 85.8789° in the RhH force field and 86.0062° in the RhH-E force field are within one degree of the average QM value, and the force constants are rather large, 5.5794 mdyn Å/rad² in the RhH force field and 4.7580 mdyn Å/rad² in the RhH-E force field. The lack of variation in bite angle in the QM data set and the resulting highly rigid angle parameter may be a source of error if a ligand with a much different bite angle is used. This error is likely to be canceled since enantiomeric excess is based on a relative energy between diastereomers, specifically the $\Delta\Delta G^\ddagger$. It is unlikely that the diastereomeric *pro-R* and *pro-S* transition states would involve drastically different ligand bite angles, and therefore any energy penalty due to ligand bite angle difference would be systematic. The rest of the angle parameters were optimized to within 5 degrees of the corresponding average QM value, and the force constants were within the range of angle force constants seen elsewhere in the MM3* force field. These additional parameters are described in detail in the Supporting Information.

Table 5. Comparison of Average Bond Lengths (Å) Between QM and MM Optimized Structures for Selected Parameters in the Transition State

bond	QM	RhH		RhH-E	
		av	rmsd	av	rmsd
Rh–O	2.22	2.23	0.00	2.22	0.01
Rh–C	2.34	2.34	0.01	2.34	0.01
Rh–P _t	2.29	2.30	0.01	2.32	0.03
Rh–P _c	2.39	2.40	0.01	2.39	0.01
Rh–H _{ax}	1.56	1.56	0.00	1.57	0.00
Rh–H _{eq}	1.63	1.64	0.02	1.66	0.03
C–C	1.42	1.45	0.03	1.45	0.03
C–H	1.71	1.63	0.08	1.61	0.10

Table 6. Comparison of Average Angle Measurements (deg) between QM and MM Optimized Structures for Selected Parameters in the Transition State

angle	QM	RhH		RhH-E	
		av	rmsd	av	rmsd
O–Rh–C	74.6	74.2	0.5	74.7	0.3
O–Rh–P _t	171.4	170.3	1.9	170.6	2.0
O–Rh–P _c	89.7	89.3	0.7	89.1	0.9
O–Rh–H _{ax}	93.0	92.9	0.5	92.3	1.1
O–Rh–H _{eq}	93.0	93.5	0.9	93.4	0.9
C–Rh–P _t	113.6	115.1	2.3	114.3	2.2
C–Rh–P _c	108.1	109.2	1.2	109.9	1.8
C–Rh–H _{ax}	162.1	161.1	1.5	160.8	1.7
C–Rh–H _{eq}	83.0	81.2	2.0	80.7	2.5
P _t –Rh–P _c	86.4	85.3	1.2	85.2	1.3
P _t –Rh–H _{ax}	79.2	78.6	1.5	79.7	1.3
P _t –Rh–H _{eq}	89.5	90.5	1.2	90.9	1.7
P _c –Rh–H _{ax}	84.2	83.8	1.4	83.3	1.8
P _c –Rh–H _{eq}	168.8	169.5	1.3	169.4	1.5
H _{ax} –Rh–H _{eq}	84.9	86.0	1.4	86.4	1.7

To include all parameters required by the program, ten torsion parameters were included in the force fields. Due to the pseudo-octahedral nature of the catalyst substructure, torsions are redundant when combined with the necessary bond and angle parameters. Furthermore, since the substrate and ligand are both bidentate in their binding, there is a lack of conformational flexibility that would require torsional parameters. The ten added torsions are all general parameters and are all set with $V_1 = V_2 = V_3 = 0.0000$, therefore not adding any torsional component to the energy of the substructure.

Comparison of QM and MM Optimized Structures.

All nine structures showed excellent agreement between the QM and MM methods with regards to the bonds and angles defined by the new parameters. The statistics for the comparisons of the average bond lengths are shown in Table 5 and average angle measurements in Table 6. For the bond lengths, the rmsd between the QM and MM structures were 0.03 Å or less for all new bonds with both force fields, except for the forming C–H bond, where the rmsd was 0.08 Å in the RhH force field and 0.10 Å in the RhH-E force field. This slightly higher error is due to the extremely large force constant described previously that results in an almost constant value of 1.63 Å in the RhH force field and 1.61 Å in the RhH-E force field compared to the QM average value of 1.71 Å. As has been discussed earlier, the Q2MM technique results in a negative response to steric crowding

Table 7. Comparison of Calculated Enthalpies (kcal/mol) between QM and MM Optimized Diastereomers and Conformers

ligand	QM	RhH	RhH-E
DMPE	−0.1	−0.3	−0.2
DuPHOS	2.3	2.1	2.2
BPE 1	2.2	2.0	2.0
BPE 2	1.9	2.5	2.4
BPE 3	3.0	2.2	2.7

of the breaking and forming bonds; the utilization of a high force constant serves to minimize the error by minimizing the bond length variation.^{4,30}

The newly defined angles generally have RMSDs under 2 degrees, with a small number of exceptions. The C–Rh–H angle averages 83.0° in the QM structures, but only 81.2° in the RhH force field with an rmsd of 2.0°, and 80.7° in the RhH-E force field with an rmsd of 2.5°. Since the forming C–H bond is systematically shorter in the MM structures than in the QM structures, it follows that that this angle would also be smaller as this angle is opposite the forming C–H bond in a four-membered ring. Two other angles with large deviations are the O–Rh–P_t and C–Rh–P_t angles that have RMSDs between 1.9° and 2.3°. These deviations result from the effect of the ligand bite angle. The P–Rh–P angle averages 86.4° in the QM structures, but a slightly smaller 85.3° from the RhH force field, and 85.2° from the RhH-E force field. Since the force constant on this angle is much larger than those on the O–Rh–P_t or C–Rh–P_t angles, the bite angle is enforced at the expense of other angles. The result is a slightly smaller O–Rh–P_t angle and a slightly larger C–Rh–P_t angle. Overall, it does not grossly distort the structures and the errors are systematic and relatively small. It is also worth noting that the parameters with zero force constants did not show any excessively large deviations. The Rh–C bond has RMSDs of 0.01 Å for both force fields, and the five angles with zero, or vanishingly small, force constants had RMSDs ranging from 0.3° to 1.7°. From these data, it can be concluded that the force constants can go to zero in the optimization due to the parameters being defined through the use of other parameters within a ring.

The accurate reproduction of the relative energies between diastereomers and conformers is very important to the predictive ability of the new force field parameters. The two force fields performed moderately well in reproducing the relative energies afforded by the training set. The relative QM enthalpies and corresponding MM energies are shown in Table 7. The RhH force field generally had poorer energy reproduction than the RhH-E force field, with an rmsd of 0.5 kcal/mol compared to 0.3 kcal/mol for the RhH-E force field. The largest unsigned error for the RhH force field was between two structures that were diastereomers utilizing the BPE ligand where the RhH force field underestimated the energy by 0.8 kcal/mol. The largest unsigned error for the RhH-E force field was half of that for the RhH force field, 0.4 kcal/mol, also for diastereomers involving the BPE ligand. The energy reproductions for the conformers of the DMPE ligand and the diastereomers of the DuPHOS ligand were under 0.2 kcal/mol for both force fields. The emphasis on energy values in the RhH-E force field is thus evident in

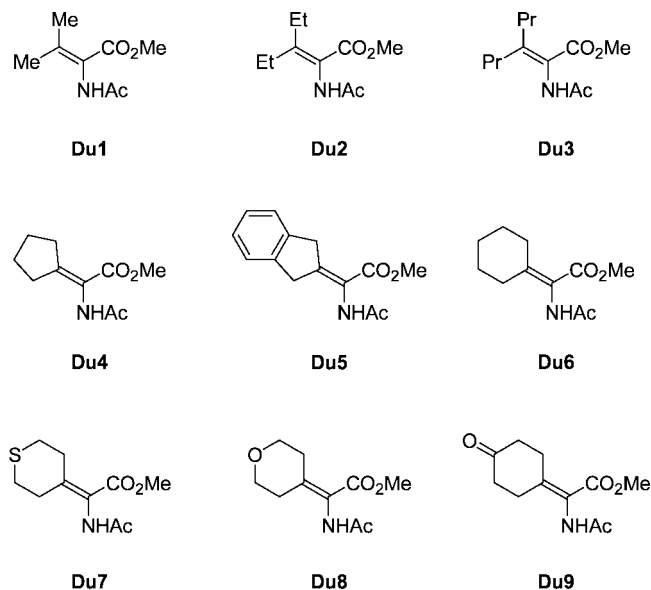


Figure 7. Substrates in the test set.

the reduction of errors in the training set. Nevertheless, the differences are fairly subtle, as can be seen in the similar optimized parameters in the two force fields. This also indicates that the optimization procedure is fairly robust at least in the present case.

Validation of the MM Parameters. Although the focus of the present manuscript is on the development rather

than the application of the force field, it is important that the optimized parameters are validated using a test set that was not part of the training set. At the same time, the number of possible data sets that were studied under identical conditions and cover a range of substrates and e.e. in the literature is surprisingly small. Finally, an ideal data set would also allow a test of how well the underlying DFT calculations reproduce the interactions in the stereodetermining transition structures, even though in the absence of conformational sampling it is not expected that they accurately reproduce the experimentally observed e.e.s. As a compromise between all these boundary conditions, we chose a data set utilizing the DuPHOS and BPE ligands and a set of dehydro- α -amino acid substrates with symmetric alkyl groups at the β position, as shown in Figure 7.³¹ The DuPHOS and BPE ligands were studied by DFT and used in the parameter optimization, but the experimentally observed e.e.s were not used in the parametrization. The substrates are not the same as the model substrate that was used in the QM training set and correspond to the substrates that would be used in a real-world study.

The computational results and reported experimental values are given as percent enantiomeric excesses, as shown in Figure 8 for the DuPHOS ligand and in Figure 9 for the BPE ligand. It can be seen in these two figures that the agreement between experimental and computa-

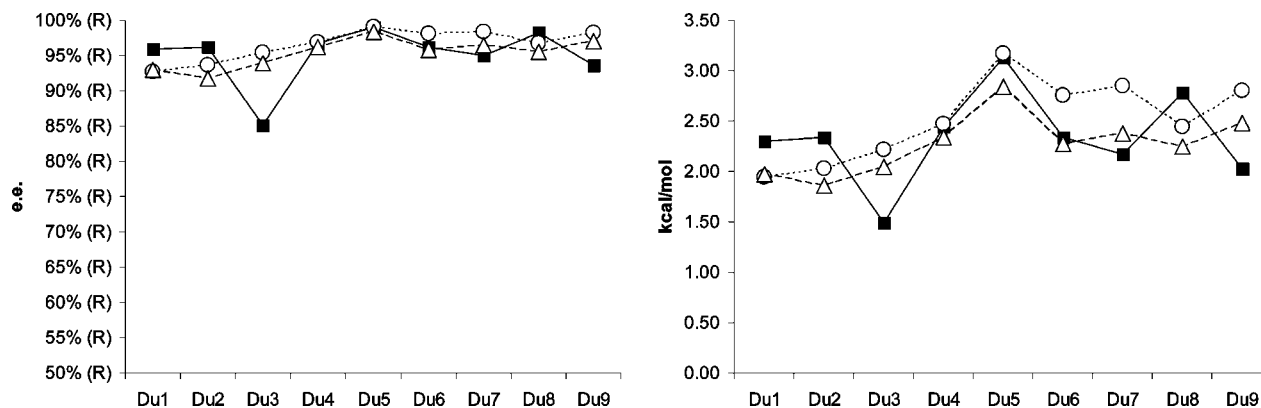


Figure 8. Comparison of computed e.e. (left) and energies (right) from the RhH force field (circles) and RhH-E force field (triangles) to experimental values (solid squares) for reactions using the DuPHOS ligand.

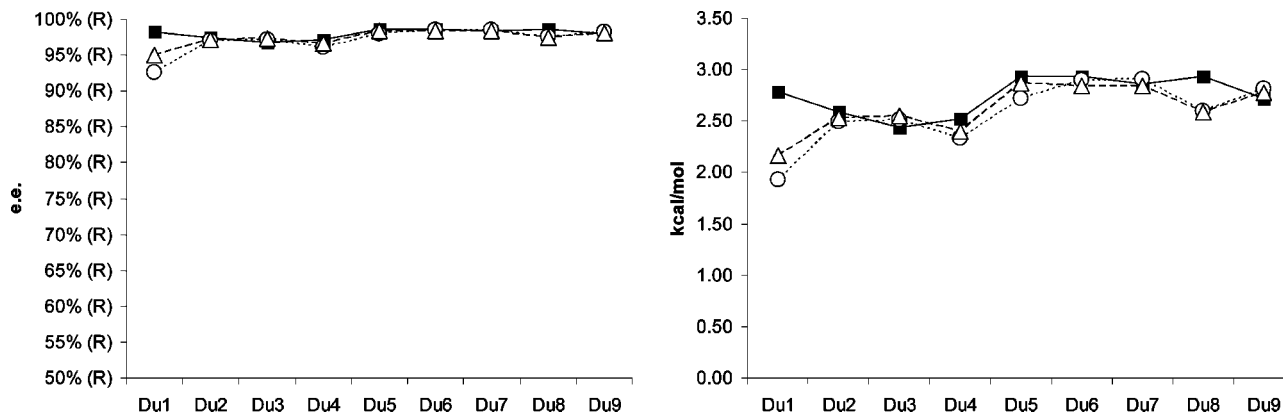


Figure 9. Comparison of computed e.e. (left) and energies (right) from the RhH force field (circles) and RhH-E force field (triangles) to experimental values (solid squares) for reactions using the BPE ligand.

tional values is very good. Because the experimentally observed e.e.s in this data set, like in most published cases, are very high, a statistical analysis in terms of e.e. is not very useful, and a discussion in terms of energies gives more insight into the performance of the method (for full listing of the energies, see tables in the Supporting Information). For the DuPHOS ligand using the RhH force field, the mean unsigned error is 0.4 kcal/mol with a maximum error of 0.7 kcal/mol, and the RhH-E force field performed slightly better with a mean unsigned error of 0.3 kcal/mol, with a maximum absolute error of 0.6 kcal/mol. The BPE ligand fared even better with a mean unsigned error of 0.2 kcal/mol for both force fields and a maximum error of 0.9 kcal/mol for the RhH force field and 0.6 kcal/mol for the RhH-E force field. The poorer performance of the DuPHOS ligand is mostly attributed to a disagreement between theory and experiment using substrate **Du3**, which is the dipropyl derivative of the substrate. This substrate gave an 85.1% e.e. experimentally, but the rest of the substrates showed e.e.s between 93.7% and 99.0%. For the chirally similar BPE ligand, **Du3** was experimentally determined to generate the reduced product in 96.8% e.e. From a statistical viewpoint, the error contributed by **Du3** is minor and does not diminish the performance of the force fields to reproduce these experimental data. Excluding this data point from the error analysis does not affect the unsigned mean error. Energetically, this point is the largest error for the DuPHOS ligand using the RhH-E force field, but the maximum unsigned error using the RhH force field is with substrate **Du9**, where the experimental e.e. of 93.7% was calculated to be a slightly higher 98.2% e.e.

Conclusions

The newly derived transition state force field parameters for the rhodium-catalyzed hydrogenation of enamides perform very well, both in comparison to the QM data and a variety of substrates. The reaction-specific force field parameters for the hydrogenation of dehydro- α -amino acid substrates with chiral bis-phosphine ligands describe the enantioselectivity of the synthesis of amino acids well and can find wide applicability to this important reaction³² but can most likely not be used for other types of reactions or substrates. The two force fields, derived from different tolerance levels of relative energies in the Q2MM method, had new parameters that were very similar to each other and, as a result, demonstrate the robustness of the fitting procedure and performed similarly as well. At the present state of development, the new parameters meet the objective stated at the outset of this work to provide a computational tool for rapid *in silico* screening of a library of ligands to identify a smaller subset for experimental screening. This goal is met, even with the small number of false positives and false negatives that arise. Nonetheless, further modifications of the parameters may lead to improved performance of this computational screening tool.

Acknowledgment. We gratefully acknowledge the allocation of computer resources by the Center for Research

Computing at the University of Notre Dame. P.J.D. is the recipient of a Schmitt Fellowship by the University of Notre Dame.

Supporting Information Available: Cartesian coordinates, imaginary frequencies, SCF energies and enthalpies of all QM transition structures calculated, expanded tables of geometric data comparing QM and MM structures, force field parameters in MacroModel format, and numerical results for Figures 8 and 9. This material is available free of charge via the Internet at <http://pubs.acs.org>.

References

- (1) (a) Burk, M. J. *Acc. Chem. Res.* **2000**, *33*, 363. (b) Genet, J.-P. *Acc. Chem. Res.* **2003**, *36*, 908. (c) Tang, W.; Zhang, X. *Chem. Rev.* **2003**, *103*, 3029. (d) Gridnev, I. D.; Imamoto, T. *Acc. Chem. Res.* **2004**, *37*, 633. (e) Cui, X.; Burgess, K. *Chem. Rev.* **2005**, *105*, 3272. (f) de Vries, J. G.; Lefort, L. *Chem. Eur. J.* **2006**, *12*, 4722. (g) Jäkel, C.; Paciello, R. *Chem. Rev.* **2006**, *106*, 2912. (h) Wu, J.; Chan, A. S. C. *Acc. Chem. Res.* **2006**, *39*, 711. (i) de Vries, J. G.; Lefort, L. *Chem. Eur. J.* **2006**, *12*, 4722. (j) Minnaard, A. J.; Feringa, B. L.; Lefort, L.; de Vries, J. G. *Acc. Chem. Res.* **2007**, *40*, 1267. (k) Zhang, W.; Chi, Y.; Zhang, X. *Acc. Chem. Res.* **2007**, *40*, 1278. (l) Johnson, N. B.; Lennon, I. C.; Moran, P. H.; Ramsden, J. A. *Acc. Chem. Res.* **2007**, *40*, 1291. (m) Roseblade, S. J.; Pfaltz, A. *Acc. Chem. Res.* **2007**, *40*, 1402.
- (2) For recent reviews, compare: (a) Shurki, A.; Warshel, A. *Adv. Protein Chem.* **2003**, *66*, 249. (b) Estiu, G.; Suárez, D.; Merz, K. M. *J. Comput. Chem.* **2006**, *27*, 1240.
- (3) Lin, H.; Truhlar, D. G. *Theor. Chem. Acc.* **2007**, *117*, 185.
- (4) (a) Norrby, P.-O. *J. Mol. Chem. (THEOCHEM)* **2000**, 506, 9. (b) Norrby, P.-O.; Brandt, P. *Coord. Chem. Rev.* **2001**, *212*, 79. (c) Jensen, F.; Norrby, P.-O. *Theor. Chem. Acc.* **2003**, *109*, 1.
- (5) DeTar, D. F.; Tenlos, C. J. *J. Am. Chem. Soc.* **1976**, *98*, 7903.
- (6) Hermann, J. C.; Marti-Arbona, R.; Fedorov, A. A.; Fedorov, E.; Almo, S. C.; Shoichet, B. K.; Rauschel, F. M. *Nature* **2007**, *448*, 775.
- (7) For a recent implementation of this approach, compare: (a) Corbeil, C. R.; Thielges, S.; Schwartzentruber, J. A.; Moitessier, N. *Angew. Chem. Int. Ed.* **2008**, *47*, 2635.
- (8) (a) Houk, K. N.; Rondan, N. G.; Wu, Y. D.; Metz, J. T.; Paddon-Row, M. N. *Tetrahedron* **1984**, *40*, 2257. (b) Houk, K. N.; Paddon-Row, M. N.; Rondan, N. G.; Wu, Y. D.; Brown, F. K.; Spellmeyer, D. C.; Metz, J. T.; Li, Y.; Loncharich, J. R. *Science* **1986**, *231*, 1108.
- (9) (a) Masamune, S.; Kennedy, R. M.; Petersen, J. S.; Houk, K. N.; Wu, Y. D. *J. Am. Chem. Soc.* **1986**, *108*, 7404. (b) Dorigo, A. E.; Houk, K. N. *J. Org. Chem.* **1988**, *53*, 1650.
- (10) Sherrod, M. J.; Menger, F. M. *J. Am. Chem. Soc.* **1989**, *111*, 2611.
- (11) Menger, F. M.; Sherrod, M. J. *J. Am. Chem. Soc.* **1990**, *112*, 8071.
- (12) (a) van Duin, A. C. T.; Dasgupta, S.; Lorant, F.; Goddard, W. A., III. *J. Phys. Chem. A* **2001**, *105*, 9396. (b) Chenoweth, K.; Duin, A. C. T.; Goddard, W. A., III. *J. Phys. Chem. A* **2008**, *112*, 1040.
- (13) (a) Strachan, A.; van Duin, A. C. T.; Chakraborty, D.; Dasgupta, S.; Goddard, W. A., III. *Phys. Rev. Lett.* **2003**, *91*, 098301. (b) Chenoweth, K.; Cheung, S.; van Duin, A. C. T.;

- Goddard, W. A., III; Kober, E. M. *J. Am. Chem. Soc.* **2005**, *127*, 7192. (c) van Duin, A. C. T.; Zeiri, Y.; Dubnikova, F.; Kosloff, R.; Goddard, W. A., III *J. Am. Chem. Soc.* **2005**, *127*, 11053. (d) Bueher, M. J.; van Duin, A. C. T.; Goddard, W. A., III *Phys. Rev. Lett.* **2006**, *96*, 095505.
- (14) (a) Jensen, F. *J. Am. Chem. Soc.* **1992**, *114*, 1596. (b) Jensen, F. *J. Comput. Chem.* **1994**, *15*, 1199. (c) Olsen, P. T.; Jensen, F. *J. Chem. Phys.* **2003**, *118*, 3523.
- (15) (a) Nielson, K. D.; van Duin, A. C. T.; Oxgaard, J.; Deng, W.-Q.; Goddard, W. A., III *J. Phys. Chem. A* **2005**, *109*, 493. (b) Han, S. S.; van Duin, A. C. T.; Goddard, W. A., III; Lee, H. M. *J. Phys. Chem. A* **2005**, *109*, 4575. (c) Zhang, Q.; Qi, Y.; Hector, L. G., Jr.; Çağın, T.; Goddard, W. A., III *Phys. Rev. B* **2005**, *72*, 045406. (d) Ludwig, J.; Vlachos, D. G.; van Duin, A. C. T.; Goddard, W. A., III *J. Phys. Chem. B* **2006**, *110*, 4274. (e) Goddard, W. A., III; van Duin, A.; Chenoweth, K.; Cheng, M.-J.; Pudar, S.; Oxgaard, J.; Merinov, B.; Jang, Y. H.; Persson, P. *Top. Catal.* **2006**, *38*, 93.
- (16) Rappé, A. K.; Casewit, C. J.; Colwell, K. S.; Goddard, W. A., III; Skiff, W. M. *J. Am. Chem. Soc.* **1992**, *114*, 10024.
- (17) For recent applications, see for example: (a) Rydberg, P.; Hansen, S. M.; Kongsted, J.; Norrby, P.-O.; Olsen, L.; Ryde, U. *J. Chem. Theory Comput.* **2008**, *4*, 673. (b) Rydberg, P.; Olsen, L.; Norrby, P.-O.; Ryde, U. *J. Chem. Theory Comput.* **2007**, *3*, 1765.
- (18) (a) Halpern, J. *Science* **1982**, *217*, 401. (b) Chua, P. S.; Roberts, N. K.; Bosnich, B.; Okrasinski, S. J.; Halpern, J. *J. Chem. Soc., Chem. Commun.* **1981**, 1278. (c) Schmidt, T.; Baumann, W.; Drexler, H.-J.; Arrieta, A.; Heller, D. *Organometallics* **2005**, *24*, 3842. (d) Reetz, M. T.; Meiswinkel, A.; Mehler, G.; Angermund, K.; Graf, M.; Thiel, W.; Mynott, R.; Blackmond, D. G. *J. Am. Chem. Soc.* **2005**, *127*, 10305.
- (19) (a) Chan, A. S. C.; Pluth, J. J.; Halpern, J. *J. Am. Chem. Soc.* **1980**, *102*, 5952. (b) Landis, C. R.; Brauch, T. W. *Inorg. Chim. Acta* **1998**, *270*, 285. (c) Landis, C. R.; Halpern, J. *J. Am. Chem. Soc.* **1987**, *109*, 1746. (d) Brown, J. M.; Parker, D. *J. Org. Chem.* **1982**, *47*, 2722. (e) Brown, J. M.; Parker, D. *Organometallics* **1982**, *1*, 950.
- (20) (a) Chen, A. S. C.; Halpern, J. *J. Am. Chem. Soc.* **1980**, *102*, 838. (b) Yasutake, M.; Gridnev, I. D.; Higashi, N.; Imamoto, T. *Org. Lett.* **2001**, *3*, 1701.
- (21) (a) Scott, J. W.; Keith, D. D.; Nix, G., Jr.; Parrish, D. R.; Remington, S.; Roth, G. P.; Townsend, J. M.; Valentine, D., Jr.; Young, R. *J. Org. Chem.* **1981**, *46*, 5086. (b) Koenig, K. E.; Knowles, W. S. *J. Am. Chem. Soc.* **1978**, *100*, 7561. (c) Detellier, C.; Gelbard, G.; Kagan, H. B. *J. Am. Chem. Soc.* **1978**, *100*, 7556.
- (22) (a) Landis, C. R.; Hilfenhaus, P.; Feldgus, S. *J. Am. Chem. Soc.* **1999**, *121*, 8741. (b) Feldgus, S.; Landis, C. R. *J. Am. Chem. Soc.* **2000**, *122*, 12714. (c) Feldgus, S.; Landis, C. R. *Organometallics* **2001**, *20*, 2374.
- (23) Donoghue, P. J.; Helquist, P.; Wiest, O. *J. Org. Chem.* **2007**, *72*, 839.
- (24) *Jaguar 5.5*; Schrödinger L.L.C.: Portland, OR, 1991–2003.
- (25) Hay, P. J.; Wadt, W. R. *J. Chem. Phys.* **1985**, *82*, 299.
- (26) (a) Chirlian, L. E.; Francl, M. M. *J. Comput. Chem.* **1987**, *8*, 894. (b) Woods, R. J.; Khalil, M.; Pell, W.; Moffat, S. H.; Smith, V. H., Jr. *J. Comput. Chem.* **1990**, *11*, 297. (c) Breneman, C. M.; Wiberg, K. B. *J. Comput. Chem.* **1990**, *11*, 361.
- (27) Mohamadi, F.; Richards, N. G. J.; Guida, W. C.; Liskamp, R.; Lipton, M.; Caufield, C.; Chang, G.; Hendrickson, T.; Still, W. C. *J. Comput. Chem.* **1990**, *11*, 440–467.
- (28) Allinger, N. L.; Yuh, Y. H.; Lii, J.-H. *J. Am. Chem. Soc.* **1989**, *111*, 8551.
- (29) Chan, A. S. C.; Pluth, J. J.; Halpern, J. *Inorg. Chim. Acta* **1979**, *37*, L477.
- (30) Norrby, P.-O.; Rasmussen, T.; Haller, J.; Strassner, T.; Houk, K. N. *J. Am. Chem. Soc.* **1999**, *121*, 10186.
- (31) Burk, M. J.; Gross, M. F.; Martinez, J. P. *J. Am. Chem. Soc.* **1995**, *117*, 9375.
- (32) For applications of this force field, see: Donoghue, P. J.; Helquist, P.; Norrby, P.-O.; Wiest, O. submitted for publication.

CT800132A